

Particle Method Simulation of Wave Impact on Structures

†M. Luo, *C.G. Koh and W. Bai

Department of Civil and Environmental Engineering, National University of Singapore, Singapore 117576

†Corresponding author: ceelm@nus.edu.sg

*Presenting author: cgkoh@nus.edu.sg

Abstract

In this paper, a Consistent Particle Method (CPM) is presented to model violent wave impact with compressible air pockets. The novelty of this method lies in four key aspects: (1) accurate computation of spatial derivatives for Laplacian and gradient operators (and hence better pressure prediction) without the use of kernel function unlike some other particle method, (2) rational treatment of density discontinuity at the water-air interface without any smoothing or smearing scheme, (3) a thermodynamics-based compressible solver for modelling compressible air that eliminates the need of determining the artificial sound speed, and (4) two-phase coupling of compressible air solver and incompressible water solver without iteration between the two solvers. An experimental study of sloshing impact with entrapped air pocket is conducted to validate the numerical model.

Keywords: Particle Method, Wave Impact, Two-phase Flow, Air Compressibility.

Introduction

Modelling of wave impact on structures is of great practical interest in offshore and marine engineering e.g. for design of seawalls against tsunami waves in terms of the required height and strength. With the rapid advances of computer power, many numerical methods have been developed to predict the wave profile and impact forces. However, most of these studies^{1, 2} do not consider the presence of entrapped air pockets, or treat the air pockets as incompressible. While incompressibility is a reasonable assumption in some water-air flow scenarios³, air entrapment or entrainment may be generated in some other problems such as violent wave impact on structures⁴. The compressibility of entrapped air pockets can play an important role in the water-air interaction in terms of influencing the pressure peak and impact duration in a wave impact process⁵. Therefore, it is necessary to include air compressibility to better simulate such water-air flow problems.

The numerical difficulties to model wave impact problems with entrapped air pockets include the large and discontinuous deformation of fluid and the abrupt discontinuity of fluid properties (density and viscosity) at the interface between water and air. A greater challenge is to have an integrated solution for water and air that behave very differently, the former being practically incompressible and the latter highly compressible. To address these issues, many mesh-based methods (such as Finite Difference Method and Finite Volume Method) and particle methods have been developed. Due to the meshless and Lagrangian nature, particle methods possess three inherent advantages over mesh-based methods: (1) better capability in modelling large and discontinuous fluid motion such as breaking waves, (2) better tracking of moving interface of different fluids, and (3) no numerical diffusion induced by the convection term in the Navier-Stokes equation. Therefore, a particle method was selected as the underlying tool of the present study. The most commonly used particle methods include SPH, ISPH, MPS and CPM. The primary difference between them lies in the computation of spatial derivatives. Compared to the other three, CPM computes the gradient and Laplacian operators in a more fundamental way by using Taylor series

expansion. Eliminating the use of a kernel function, the spatial derivatives can be approximated much more accurately and hence no artificial schemes are required⁶.

The main difficulties of using CPM to simulate violent waves with air entrapment is the approximation of spatial derivatives with sharp density change across fluid interface and the consistent modelling of incompressible water and compressible air. To address these two issues, an improvement of the derivative-approximation scheme in the original CPM was recently proposed to deal with the sharp density discontinuity⁶. In addition, a thermodynamically-consistent compressible solver that not only can be integrated with the developed incompressible solver seamlessly but also can overcome some issues encountered by other compressible solvers is developed⁷. In this paper, the main features and advantages of CPM are presented systematically. Using this method, water sloshing with entrapped air pocket in a specially designed oscillating tank is studied with our own experimental validation.

Governing equations and CPM formulations

The governing equations for viscous Newtonian fluids (both incompressible and compressible) in a two-fluid system are the Navier-Stokes equations as follows⁸:

$$\frac{1}{\rho} \frac{D\rho}{Dt} + \nabla \cdot \mathbf{v} = 0 \quad (1)$$

$$\frac{D\mathbf{v}}{Dt} = -\frac{1}{\rho} \nabla p + \frac{1}{\rho} \nabla \cdot \left[\mu \left(\nabla \mathbf{v} + (\nabla \mathbf{v})^T \right) \right] + \mathbf{g} \quad (2)$$

where ρ is the density of fluid, \mathbf{v} the particle velocity vector, p the fluid pressure, μ the dynamic viscosity of fluid and \mathbf{g} the gravitational acceleration.

For both incompressible and compressible fluids, the governing equations are solved by a predictor-corrector scheme^{9, 10}. In the predictor step, the temporary particle velocities and positions are computed by neglecting the pressure gradient term. In the corrector step, a pressure Poisson equation (PPE) can be derived as follows

$$\nabla \cdot \left(\frac{1}{\rho^*} \nabla p^{(k+1)} \right) = \frac{1}{\Delta t^2} \frac{\rho^{(k+1)} - \rho^*}{\rho^{(k+1)}} \quad (3)$$

For incompressible fluids, the incompressibility condition is enforced by setting the fluid density at the current time step ($\rho^{(k+1)}$) to the initial value (ρ_0). The intermediate fluid density (ρ^*) is evaluated in the same way introduced in Luo et al.⁶. For compressible fluids, although a similar approach is used to evaluate fluid density, a slow-slope weighting functions whose value at $r = 0$ is smaller is adopted to allow more compressibility of fluid (more details can be referred to Luo et al.⁷). Another distinct feature in the simulation of compressible flows is that, without the incompressibility condition, the fluid density $\rho^{(k+1)}$ in Equation (3) should be treated as unknown (more details will be presented later).

Gradient and Laplace operators involving density discontinuity

The derivative computation scheme in CPM is derived based on Taylor series expansion. This scheme has been demonstrated to work well for 1-phase flows^{11, 12}. In two-phase flows, the pressure function is continuous at the fluid interface but its gradient changes drastically because of the large density difference between two fluids (e.g. water and air densities differ by three orders of magnitude)⁶. Hence, when applied to pressure, the scheme introduced in the previous section does

not give good approximation of gradient and Laplacian terms near the fluid interface. This problem, nevertheless, can be resolved by observing that the pressure gradient normalized with respect to density, i.e. $\nabla p / \rho$, is of the same order of magnitude in the two fluids of a general dynamic problem and, in the hydrostatic case, is in fact constant. By addressing the normalized pressure gradient term, the formulation to compute the gradient and Laplacian operators with abrupt density discontinuity can be derived to be (more details can be referred to Luo et al. ⁶)

$$\left(\frac{1}{\rho} \frac{\partial p}{\partial x} \right)_i = \sum_{j \neq i} \left[\frac{1}{0.5(\rho_i + \rho_j)} C_{1j} (p_j - p_i) \right] \quad (4)$$

and

$$\left(\frac{\partial}{\partial x} \left(\frac{1}{\rho} \frac{\partial p}{\partial x} \right) \right)_i = \sum_{j \neq i} \left[\frac{1}{0.5(\rho_i + \rho_j)} C_{3j} (p_j - p_i) \right] \quad (5)$$

The coefficients C_{1j} and C_{3j} are the same as those in 1-phase CPM¹¹. The above reformulation retains the consistency with Taylor series expansion in computing the required gradient and Laplace terms with abrupt density discontinuity. Since no density smoothing or smearing scheme is needed, this scheme is able to model sharp fluid interface (e.g. water and air whose density difference is about three orders of magnitude) with good accuracy.

Compressible solver based on thermodynamics

For compressible flows, $\rho^{(k+1)}$ in Equation (3) is unknown and hence a closure condition is needed to solve the PPE. The polytropic gas law as shown in Equation (4) is selected to be the closure relation since it does not require the input of speed of sound (c_s), which is dependent on the composition and temperature of a fluid. This avoids the need to determine the actual or numerical sound speed, unlike in the c_s dependent EOS.

$$\frac{P}{\rho^\gamma} = \text{constant} \quad (4)$$

where γ is the ratio of specific heats at constant pressure and constant volume. Its value for air is about 1.4.

Incorporating the closure condition of Equation (4) to Equation (3), the PPE accounting for fluid compressibility can be obtained as (more details can be referred to Luo et al. ⁷)

$$-\nabla \cdot \left(\frac{1}{\rho_i^*} \nabla p_i^{(k+1)} \right) + \frac{1}{\Delta t^2} \frac{\rho_{a0}}{\rho_i^*} \frac{1}{p_{a0}} \frac{1}{\gamma} p_i^{(k+1)} = -\frac{1}{\Delta t^2} \frac{\rho_{a0} - \rho_i^*}{\rho_i^*} + \frac{1}{\Delta t^2} \frac{\rho_{a0}}{\rho_i^*} \frac{1}{\gamma} \quad (5)$$

Since the speed of sound c_s is not involved in Equation (5), the issue of how to determine the actual or numerical value of c_s is avoided. This is a significant benefit of the present compressible solver. More importantly, this thermodynamically-consistent compressible solver and the previously proposed incompressible solver⁶ both use the predictor-corrector scheme to solve the same governing equations and thus can be easily integrated, leading to the complete two-phase model. Named 2-phase CPM, it is capable of simultaneously and consistently simulating two-phase incompressible and compressible flows with large density difference.

Numerical examples

Sloshing impact with entrapped air pocket

To study wave impact scenario with entrapped air pocket, a new experiment is designed and conducted as shown in Figure 1. The water container comprises a big (left) tank connected by a short channel to a small (right) tank. It is designed such that when water in the left tank sloshes to the right (or left), some water will move through the connecting channel and compress (or expand) the air in the right tank. The same tank as shown in Figure 16 of Luo et al.⁷ is used. Air pressure at the middle of the top wall of the right tank, i.e. P_{A1} , is measured by an absolute pressure sensor. Water pressures at 60 mm from the bottom on the right wall of the right tank (P_{W1}) and 30 mm from the bottom on the left wall of the left tank (P_{W3}) are measured by gauge pressure sensors.

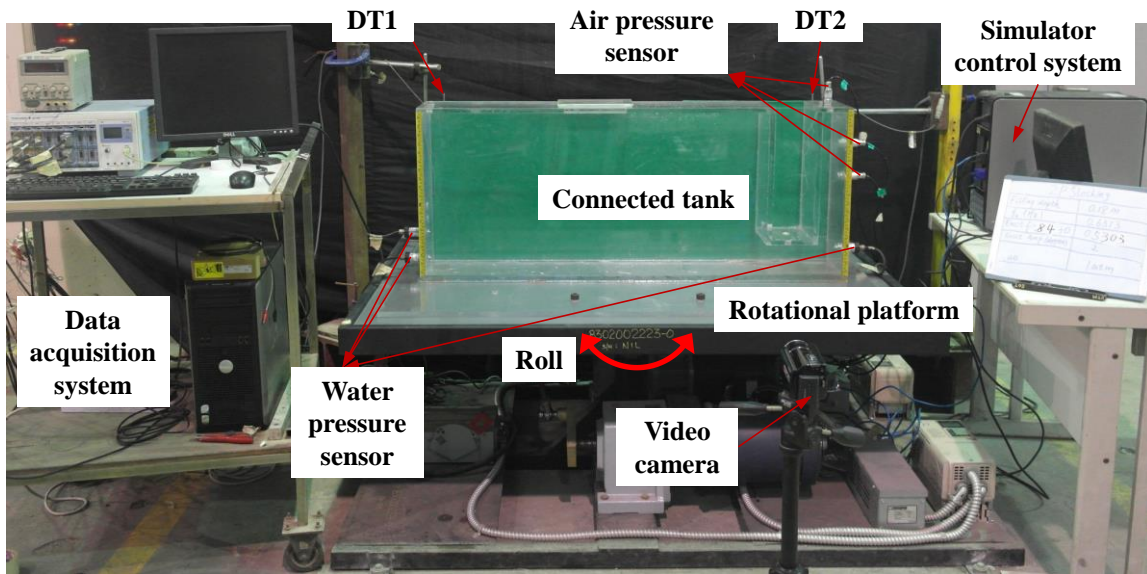
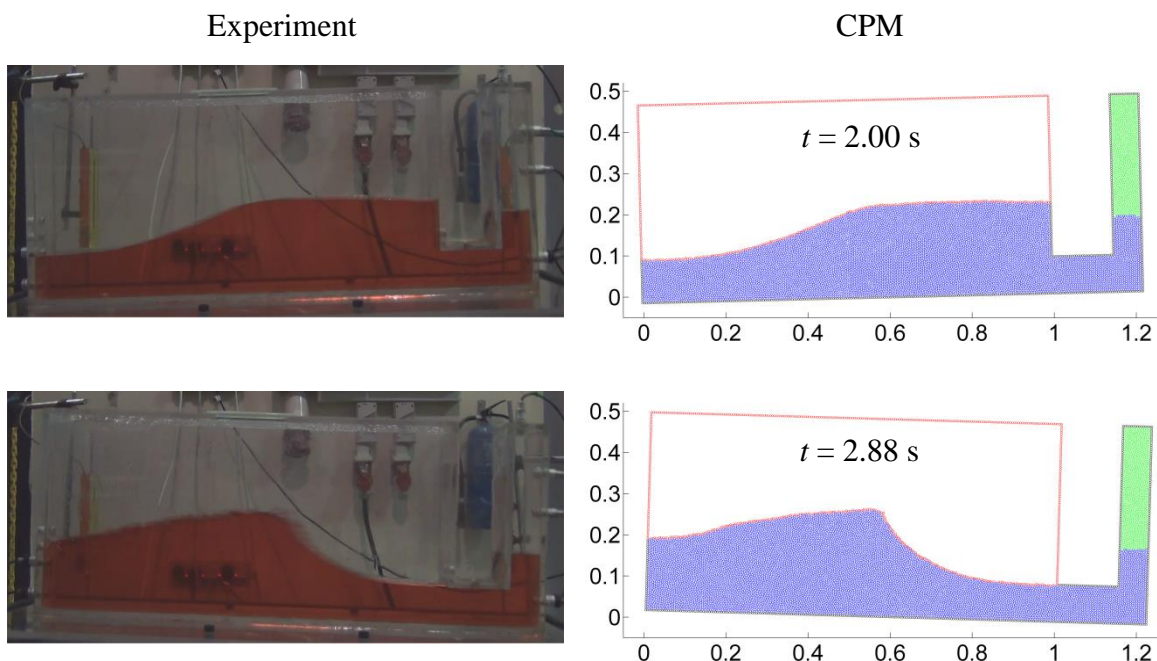


Figure 1. Setup of water-air sloshing experiments in a connected container under rotational excitation



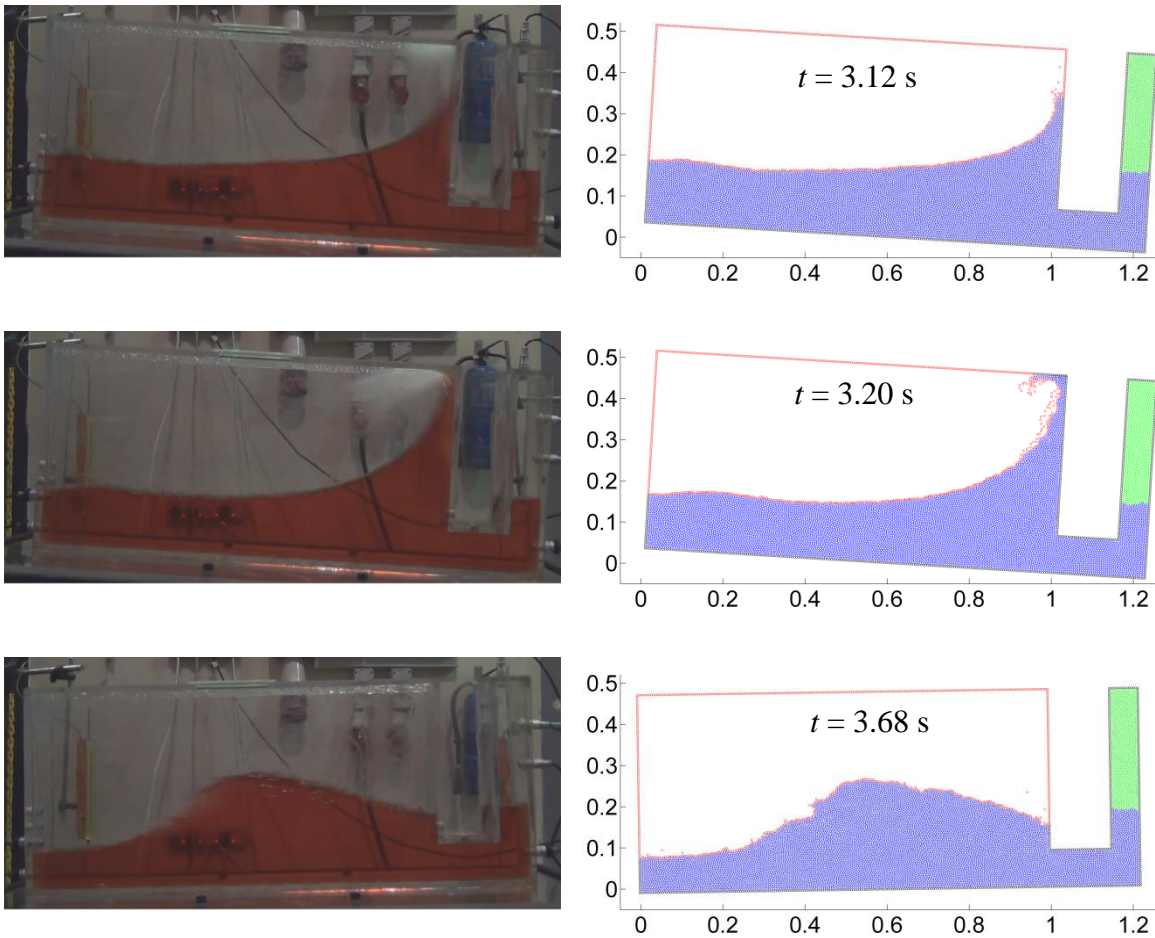


Figure 2. Wave profiles of sloshing in a connected tank with closed air pocket under rotational excitation: experimental result and CPM simulation

In the case presented in this section, the filling depth is adopted to be 0.18 m. The excitation frequency of $0.92\omega_0$ ($= 3.6493$ rad/s) is found to generate a relatively large variation of air pressure in the right tank, where ω_0 is the reference frequency (not the natural frequency of the sloshing system but only a reference value) computed based on the linear wave theory with water depth (d_L) and length (L_L) in the left tank. In numerical simulation, an initial particle distance of 0.005 m and fixed time step 0.0005 s are adopted on the tradeoff between accuracy and efficiency. The water and air densities at the NTP (Normal Temperature and Pressure) condition are adopted. The dynamic viscosities of water and air are selected to be 10^{-3} Pa s and 1.983×10^{-5} Pa s respectively.

The wave profiles and pressure histories at points A_1 , W_1 and W_3 are presented in Figure 2 and Figure 3. Generally good agreement between numerical simulation and experimental result is obtained. The water moves like a bore (because of the relatively low filling depth) which develops over time (see $t = 2.00$ s and 2.88 s in Figure 2). At $t = 3.12$ s, violent wave impact occurs near the connecting channel, generating large compression force to the air pocket in the right tank. This can be clearly seen in Figure 3a, which shows a large peak for the air pressure at point A_1 . As the water in the left tank runs up along the right wall of the left tank ($t = 3.20$ s in Figure 2), the compression force continues to exert on the air pocket in the right tank. At $t = 3.68$ s, the run-up water falls back to the water body and begins to move towards left. It is noted that the air pressure in the right tank shows vibration during the impact process. The air

pressure also influences the water pressure near the air pocket (see the water pressure at Pw1 as shown in Figure 3b).

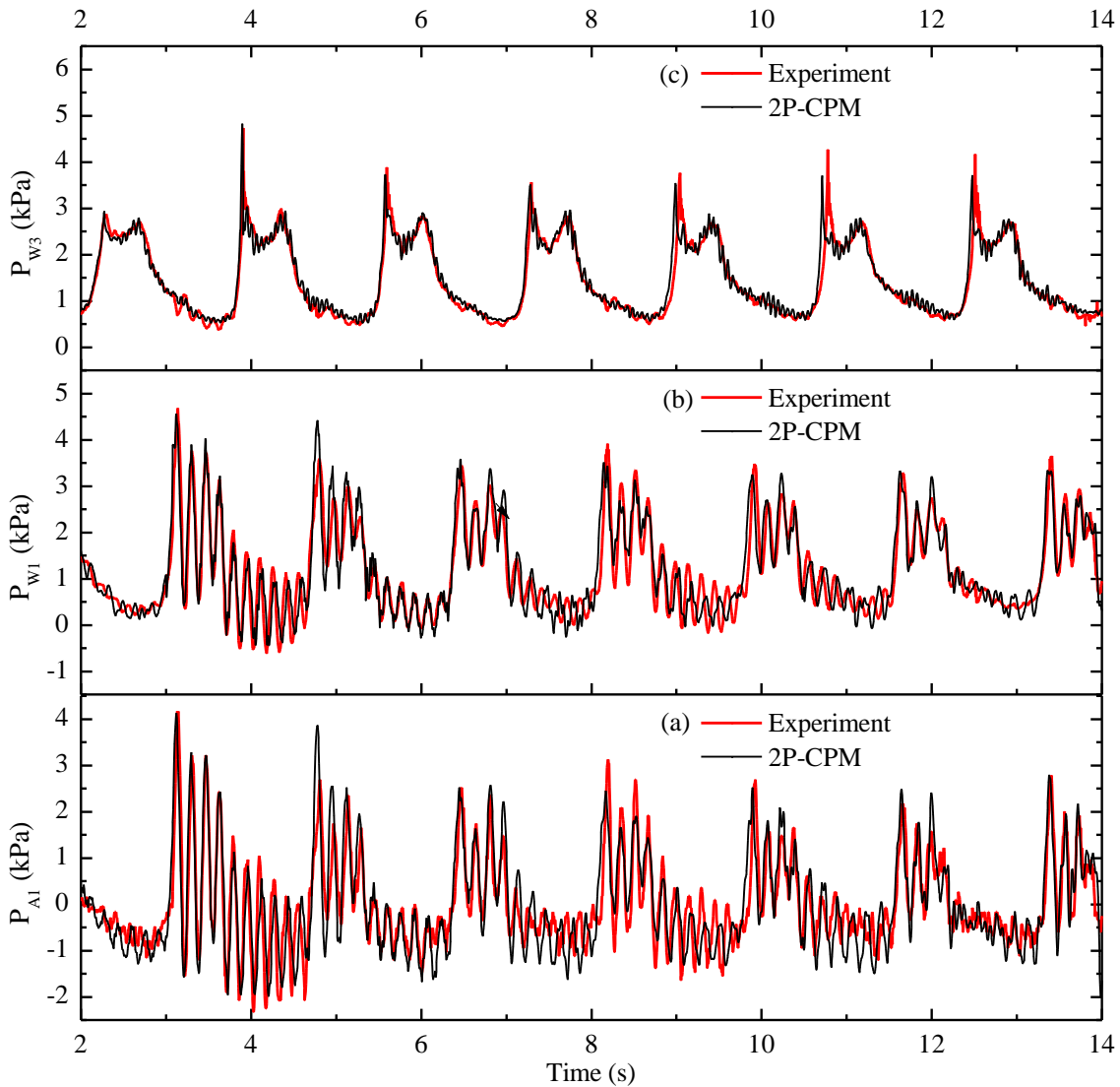


Figure 3. Simulated air pressure at Point P_{A1} and water pressures at Point P_{W1} and P_{W3} in comparison with experimental results

The pressure vibration in the air pocket is further investigated through a power spectral analysis using the Fast Fourier Transform (FFT). It is interesting to note that there is only one peak value, i.e. 6.120 Hz, in the frequency-power curve. It means that the air pressure vibrates with one distinctive frequency. To verify that this pressure vibration is real and not spurious due to the numerical algorithm, the natural frequency of the air tube (under the compression of water) is derived. Following Ramkema¹³ who addressed the problem of wave impact on coastal structures, the air-pocket-water system is represented by a mass-spring system as shown in Figure 4, in which the spring is the air pocket and the mass is the water effectively contributing to the impact. The upper bound of the effective water mass is the water in the connecting channel and the right tank, while the lower bound is the upper bound excluding the water in the rectangular region at the right bottom corner of the container (the region within the dash-dot line in Figure 4). Since water at the right bottom corner (dark shaded region in Figure 4) is almost stationary relative to the tank (theoretically the right bottom point of the container is a stagnation point), the effective mass of the present problem (light shaded region in Figure 4) is

approximated to be water in the connecting channel and the right tank excluding the right bottom corner.

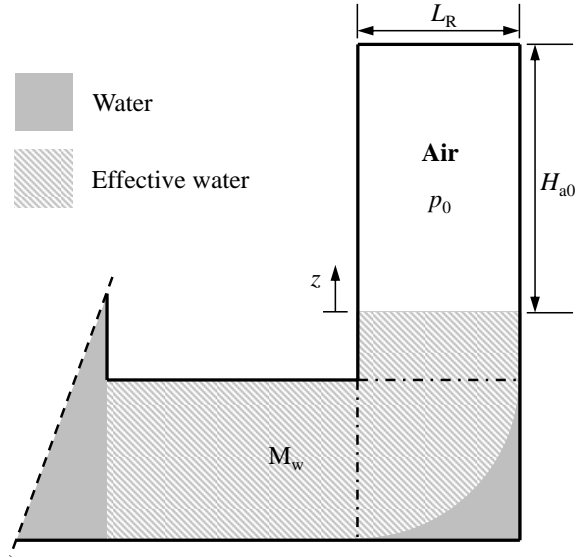


Figure 4. Schematic view of water impact on an air pocket (not to scale)

Assuming the water level in the right tank to be horizontal and giving it a small perturbation z , the force (per unit width) applied on the effective water mass is as follows

$$\begin{aligned}
 F &= (p_{a0} - p)L_R = \left[1 - \left(1 + \frac{z}{H_{a0} - z} \right)^\gamma \right] p_{a0} L_R \\
 &\approx \left[1 - \left(1 + \gamma \frac{z}{H_{a0} - z} \right) \right] p_{a0} L_R = -\frac{\gamma p_{a0} L_R}{H_{a0} - z} z \approx -\frac{\gamma p_{a0} L_R}{H_{a0}} z
 \end{aligned} \tag{6}$$

where p_{a0} is the initial air pressure in the right tank, L_R the length of the right tank and H_{a0} the initial height of the air tube. Ignoring the friction forces from the tank walls, the dynamic equation for the effective water mass is as follows

$$M_w \frac{d^2 z}{dt^2} + \frac{\gamma p_{a0} L_R}{H_{a0}} z = 0 \tag{7}$$

where M_w is the effective water mass (per unit width). Then the natural frequency of the dynamic system can be obtained as

$$f = \frac{1}{2\pi} \sqrt{\frac{\gamma p_{a0} L_R}{H_{a0} M_w}} \tag{8}$$

the form of which is similar to that derived by Cuomo *et al.*¹⁴ who analytically studied wave impingement entrapping an air pocket against vertical wall. Substituting the upper and lower bounds of M_w into Equation (8), the lower and upper bounds of the natural frequency of the entrapped air pocket can be obtained to be 5.668 Hz and 6.507 Hz, whereas the natural frequency corresponding to the adopted value of M_w is 6.296 Hz. Compared to the observed frequency of pressure vibration (i.e. 6.120 Hz) in the experimental result, the relative differences are only 7.3 %, 6.3 % and 2.8 %, respectively, for the lower and upper bounds and the adopted value of M_w . Therefore, the accuracy of this simplified model is acceptable. The study on the natural frequency

of the air pocket further substantiates that the pressure oscillations observed in the experiment and CPM simulation are real and due to the natural vibration of the entrapped air pocket (air cushion effect).

Conclusions

In this paper, the novel CPM is presented with three features: (1) Accurate computation of first- and second-order derivatives in a way consistent with Taylor series expansion even in two-phase cases with abrupt density change to about 1000; (2) A thermodynamically-consistent compressible solver by employing the polytropic gas law; (3) Seamless integration of the incompressible and compressible solvers such that wave impact problems with entrapped air pocket can be simulated in a simultaneous way.

An experimental study of water sloshing in a specially designed tank is conducted to measure the pressure change of a closed air pocket under wave impact. Numerical results including wave profiles, wave impact pressures and particularly the pressure vibration in the air pocket predicted by CPM agree generally well with the experimental results.

Acknowledgement

The authors appreciate the research grant provided by the Singapore Maritime Institute (Project SMI-2014-OF-02) as well as the funding and technical support of Sembcorp Marine Technology Pte Ltd.

References

- [1] Liu D, Lin P. A numerical study of three-dimensional liquid sloshing in tanks. *Journal of Computational Physics* 2008;227:3921-39.
- [2] Wang Y, Shu C, Huang HB, Teo CJ. Multiphase lattice Boltzmann flux solver for incompressible multiphase flows with large density ratio. *Journal of Computational Physics* 2015;280:404-23.
- [3] Heyns JA, Malan AG, Harms TM, Oxtoby OF. A weakly compressible free-surface flow solver for liquid-gas systems using the volume-of-fluid approach. *Journal of Computational Physics* 2013;240:145-57.
- [4] Peregrine DH. Water-wave impact on walls. *Annual Review of Fluid Mechanics* 2003;35:23-43.
- [5] Abrahamsen BC, Faltinsen OM. The effect of air leakage and heat exchange on the decay of entrapped air pocket slamming oscillations. *Physics of Fluids* 2011;23:102107.
- [6] Luo M, Koh CG, Gao M, Bai W. A particle method for two-phase flows with large density difference. *International Journal for Numerical Methods in Engineering* 2015;103:235-55.
- [7] Luo M, Koh CG, Bai W, Gao M. A particle method for two-phase flows with compressible air pocket. *International Journal for Numerical Methods in Engineering* 2016:n/a-n/a.
- [8] Tofighi N, Yildiz M. Numerical simulation of single droplet dynamics in three-phase flows using ISPH. *Computers & Mathematics with Applications* 2013;66:525-36.
- [9] Shao S, Lo EYM. Incompressible SPH method for simulating Newtonian and non-Newtonian flows with a free surface. *Advances in Water Resources* 2003;26:787-800.
- [10] Koshizuka S, Nobe A, Oka Y. Numerical analysis of breaking waves using the moving particle semi-implicit method. *International Journal for Numerical Methods in Fluids* 1998;26:751-69.
- [11] Koh CG, Gao M, Luo C. A new particle method for simulation of incompressible free surface flow problems. *International Journal for Numerical Methods in Engineering* 2012;89:1582-604.
- [12] Koh CG, Luo M, Gao M, Bai W. Modelling of liquid sloshing with constrained floating baffle. *Computers & Structures* 2013;122:270-9.
- [13] Ramkema C. A model law for wave impacts on coastal structures. *Coastal Engineering Proceedings* 1978.
- [14] Cuomo G, Allsop W, Takahashi S. Scaling wave impact pressures on vertical walls. *Coastal Engineering* 2010;57:604-9.